

Characteristic temperature for the immiscible-miscible transition of binary condensates in optical lattices

K. Suthar^{1,2} and D. Angom^{1,*}¹*Physical Research Laboratory, Navrangpura, Ahmedabad-380009, Gujarat, India*²*Indian Institute of Technology, Gandhinagar, Ahmedabad-382424, Gujarat, India*

(Received 23 August 2016; published 4 April 2017)

We study two-species Bose-Einstein condensates confined in quasi-two-dimensional (quasi-2D) optical lattices at finite temperatures, employing the Hartree-Fock-Bogoliubov theory with the Popov approximation. We examine the role of thermal fluctuations in the ground-state density distributions and the quasiparticle mode evolution. At zero temperature, the geometry of the ground state in the immiscible domain is side by side. Our results show that the thermal fluctuations enhance the miscibility of the condensates, and at a characteristic temperature the system becomes miscible with rotationally symmetric overlapping density profiles. This immiscible-miscible transition is accompanied by a discontinuity in the excitation spectrum, and the low-lying quasiparticle modes such as slosh mode become degenerate at the characteristic temperature.

DOI: [10.1103/PhysRevA.95.043602](https://doi.org/10.1103/PhysRevA.95.043602)

I. INTRODUCTION

Ultracold atoms in an optical lattice offer fascinating prospects to investigate many-body quantum physics of strongly correlated systems in a highly controllable environment [1–4]. These systems are recognized as ideal tools to explore new quantum phases [5–7], complex phase transitions [8–11], quantum magnetism [12,13], and quantum information [14] and to simulate the transport and magnetic properties of condensed-matter systems [15,16]. Moreover, the effects of phase separation [17,18], quantum emulsions and coherence properties [19–21], and multicritical behavior [22,23] of the mixtures have been explored in the past decade.

Among the various observations made in two-species Bose-Einstein condensates (TBECs) of ultracold atomic gases, the most remarkable is the phenomenon of phase separation, and it has been a long-standing topic of interest in chemistry and physics. For repulsive on-site interactions, the transition to the phase-separated domain or immiscibility is characterized by the parameter $\Delta = U_{11}U_{22}/U_{12}^2 - 1$, where U_{11} and U_{22} are the intraspecies on-site interactions and U_{12} is the interspecies on-site interaction. When $\Delta < 0$, an immiscible phase occurs in which the atoms of species 1 and 2 show relatively strong repulsion, whereas $\Delta \geq 0$ implies a miscible phase [24–26]. It is important to note that the mention criterion is valid at zero temperature for homogeneous systems. The presence of an external trapping potential, however, modifies this condition, as the trap introduces an additional energy cost for the species to spatially separate [27]. In experiments, the unique feature of phase separation has been successfully observed in TBECs with a harmonic trapping potential [28–30]. Previously, in the context of superfluid helium at zero temperature, the phase separation of bosonic mixtures of isotopes of different masses has also been predicted in Refs. [31] and [32]. Recent experimental realizations of TBECs in optical lattices, either of two atomic species [33] or two hyperfine states of same atomic species [34,35], provide the motivation to study these systems in detail. In recent works, we have examined the

miscible-immiscible transition, and the quasiparticle spectra of the TBECs at zero temperature in quasi-one-dimensional (quasi-1D) [36] and quasi-two-dimensional (quasi-2D) [37] geometries. The finding in the latter work [37], where we examined the nature of the density profiles in the immiscible regime at zero temperature, is of relevance to the present work. In addition, we showed how the optical lattice potential influences the density profiles in the immiscible domain. The other related study is the ground-state phase diagram, and the effect of the filling factor of the TBECs on the phenomenon of phase separation, which was investigated using quantum Monte Carlo simulations [38,39]. In addition, phase separation of TBECs at various length scales has been examined using the multiorbital mean-field theory [40,41]. Among the full quantum methods the multiconfigurational time-dependent Hartree for bosons (MCTDHB) method provides a good description of the formation of interference fringes in the densities during the mixing of condensates [42,43]. This method allows the dynamical creation of quantum superposition of states in ultracold Bose gases [44]. In other theoretical studies, the finite-temperature properties of TBECs have been explored [45–47]. In continuum or TBECs with a harmonic confining potential alone, we have explored the suppression of phase separation due to the presence of thermal fluctuations [48]. However, a theoretical understanding of the finite-temperature effects on the topology and the collective excitations of TBECs in optical lattices is yet to be explored. Bose-Einstein condensation and, hence, the coherence in a system of bosons depend on the interplay between various parameters, such as the temperature, interaction strength, confinement, and dimensionality [49]. In particular, in low-dimensional Bose gases, coherence can only be maintained across the entire spatial extent at a temperature much below the critical temperature. The coherence property, in experiments, has been studied in recent works [50–54].

With attention to this unexplored physics, we study the finite-temperature effects of quasi-2D trapped TBECs in optical lattices. In the present work, we address the topological phase transition in TBECs of two isotopes of Rb with temperature as a control parameter in the domain $T < T_c$, where T_c is the critical temperature of either of the species of

*angom@prl.res.in

the mixture. Here, it must be mentioned that in our previous works [36,37], we investigated the ground-state density and quasiparticles with variation in the on-site interaction energy at zero temperature. In addition, we have examined the effect of quantum fluctuations on the ground-state geometry and collective excitations of quasi-1D TBECs. In the present work, we examine the evolution of quasiparticle modes of TBECs in quasi-2D optical lattices with variation in the temperature. For this work, we use the Hartree-Fock-Bogoliubov (HFB) formalism with the Popov approximation, and starting from the phase-separated domain at zero temperature we increase the temperature. We observe that there is an immiscible-to-miscible transition of the TBEC at a characteristic temperature. This transition is accompanied by a discontinuity in the quasiparticle excitation spectrum, and in addition, some of the modes like the slosh mode become degenerate. We then compute the equal-time first-order spatial correlation function, which is a measure of the coherence and phase fluctuations present in the system. It describes the off-diagonal long-range order, which is a defining feature of the BEC [55]. This is an important theoretical tool to study many-body effects in atomic physics experiments [56,57].

This paper is organized as follows. In Sec. II we describe the HFB-Popov formalism and the numerical techniques used in the present work. The evolution of the quasiparticle modes and density distributions with the temperature is reported in Sec. III. Finally, our main results are summarized in Sec. IV.

II. THEORY AND METHODS

A. HFB-Popov approximation for a quasi-2D TBEC

We consider a TBEC confined in an optical lattice with a pancake-shaped configuration of the background harmonic trapping potential. Thus, the trapping frequencies satisfy the condition $\omega_{\perp} \ll \omega_z$ with $\omega_x = \omega_y = \omega_{\perp}$. In this system, the excitation energies along the axial direction are high, and the degree of freedom in this direction is frozen. The excitations, both quantum and thermal fluctuations, are considered only along the radial direction. In the tight-binding approximation [58,59], the Bose-Hubbard (BH) Hamiltonian [60–62] describing this system is

$$\hat{H} = \sum_{k=1}^2 \left[-J_k \sum_{\langle \xi \xi' \rangle} \hat{a}_{k\xi}^{\dagger} \hat{a}_{k\xi'} + \sum_{\xi} (\epsilon_{\xi}^{(k)} - \mu_k) \hat{a}_{k\xi}^{\dagger} \hat{a}_{k\xi} \right] + \frac{1}{2} \sum_{k=1, \xi}^2 U_{kk} \hat{a}_{k\xi}^{\dagger} \hat{a}_{k\xi}^{\dagger} \hat{a}_{k\xi} \hat{a}_{k\xi} + U_{12} \sum_{\xi} \hat{a}_{1\xi}^{\dagger} \hat{a}_{1\xi} \hat{a}_{2\xi}^{\dagger} \hat{a}_{2\xi}, \quad (1)$$

where $k = 1, 2$ is the species index, μ_k is the chemical potential of the k th species, and $\hat{a}_{k\xi}$ ($\hat{a}_{k\xi}^{\dagger}$) is the annihilation (creation) operators of the two species at the ξ th lattice site. The index is such that $\xi \equiv (i, j)$, with i and j the lattice site index along the x and y directions, respectively. The summation index $\langle \xi \xi' \rangle$ represents the sum over the nearest neighbor to the ξ th site. The tight-binding approximation is valid when the depth of the lattice potential is much larger than the chemical potential $V_0 \gg \mu_k$; the BH Hamiltonian then describes the system when the bosonic atoms occupy the lowest energy band. A detailed derivation of the BH Hamiltonian is given in our previous works [36,37]. In the BH Hamiltonian, J_k

are the tunneling matrix elements, $\epsilon_{\xi}^{(k)}$ is the offset energy arising due to the background harmonic potential, and U_{kk} (U_{12}) are the intraspecies (interspecies) interaction strengths. In the present work all the interaction strengths are considered to be repulsive, that is, $U_{kk}, U_{12} > 0$.

In the weakly interacting regime, under the Bogoliubov approximation [63,64], the annihilation operators at each lattice site can be written as $\hat{a}_{1\xi} = (c_{\xi} + \hat{\phi}_{1\xi})e^{-i\mu_1 t/\hbar}$ and $\hat{a}_{2\xi} = (d_{\xi} + \hat{\phi}_{2\xi})e^{-i\mu_2 t/\hbar}$, where c_{ξ} and d_{ξ} are the complex amplitudes describing the condensate phase of each of the species. The operators $\hat{\phi}_{1\xi}$ and $\hat{\phi}_{2\xi}$ represent the quantum or thermal fluctuation part of the field operators. Furthermore, we consider the system in the superfluid domain where the mean-field description is applicable, and accordingly, the parameters satisfy the condition $U/J \ll 16.7$ [65–67]. In this domain, the equation of motion of the condensate in an optical lattice with the tight-binding approximation is reduced to the discrete nonlinear Schrödinger equation (DNLSE). However, in the Mott-insulator phase, $U/J \geq 16.7$, the mean-field description breaks down, and a full quantum description is required [68–70]. From the equation of motion of the field operators with the Bogoliubov approximation, the equilibrium properties of a TBEC is governed by the coupled generalized DNLSes,

$$\mu_1 c_{\xi} = -J_1 \sum_{\xi'} c_{\xi'} + [\epsilon_{\xi}^{(1)} + U_{11}(n_{1\xi}^c + 2\tilde{n}_{1\xi}) + U_{12}n_{2\xi}^c]c_{\xi}, \quad (2a)$$

$$\mu_2 d_{\xi} = -J_2 \sum_{\xi'} d_{\xi'} + [\epsilon_{\xi}^{(2)} + U_{22}(n_{2\xi}^c + 2\tilde{n}_{2\xi}) + U_{12}n_{1\xi}^c]d_{\xi}, \quad (2b)$$

where $n_{1\xi}^c = |c_{\xi}|^2$ and $n_{2\xi}^c = |d_{\xi}|^2$, $\tilde{n}_{k\xi} = \langle \hat{\phi}_{k\xi}^{\dagger} \hat{\phi}_{k\xi} \rangle$, and $n_{k\xi} = n_{k\xi}^c + \tilde{n}_{k\xi}$ are the condensate, noncondensate, and total density of the species, respectively. The fluctuation operators are defined in terms of the quasiparticles through the Bogoliubov transformation

$$\hat{\phi}_{k\xi} = \sum_l [u_{k\xi}^l \hat{\alpha}_l e^{-i\omega_l t} - v_{k\xi}^{*l} \hat{\alpha}_l^{\dagger} e^{i\omega_l t}], \quad (3)$$

where $\hat{\alpha}_l$ ($\hat{\alpha}_l^{\dagger}$) are the quasiparticle annihilation (creation) operators, which satisfy the Bose commutation relations, l is the quasiparticle mode index, $u_{k\xi}^l$ and $v_{k\xi}^l$ are the quasiparticle amplitudes for the k th species, and $\omega_l = E_l/\hbar$ is the frequency of the l th quasiparticle mode with E_l as the mode excitation energy.

Using the Bogoliubov transformation, we obtain the HFB-Popov equations [37]

$$E_l u_{1,\xi}^l = -J_1 (u_{1,\xi-1}^l + u_{1,\xi+1}^l) + \mathcal{U}_1 u_{1,\xi}^l - U_{11} c_{\xi}^2 v_{1,\xi}^l + U_{12} c_{\xi} (d_{\xi}^* u_{2,\xi}^l - d_{\xi} v_{2,\xi}^l), \quad (4a)$$

$$E_l v_{1,\xi}^l = J_1 (v_{1,\xi-1}^l + v_{1,\xi+1}^l) + \mathcal{U}_1 v_{1,\xi}^l + U_{11} c_{\xi}^{*2} u_{1,\xi}^l - U_{12} c_{\xi}^* (d_{\xi} v_{2,\xi}^l - d_{\xi}^* u_{2,\xi}^l), \quad (4b)$$

$$E_l u_{2,\xi}^l = -J_2 (u_{2,\xi-1}^l + u_{2,\xi+1}^l) + \mathcal{U}_2 u_{2,\xi}^l - U_{22} d_{\xi}^2 v_{2,\xi}^l + U_{12} d_{\xi} (c_{\xi}^* u_{1,\xi}^l - c_{\xi} v_{1,\xi}^l), \quad (4c)$$

$$E_l v_{2,\xi}^l = J_2 (v_{2,\xi-1}^l + v_{2,\xi+1}^l) + \mathcal{U}_2 v_{2,\xi}^l + U_{22} d_{\xi}^{*2} u_{2,\xi}^l - U_{12} d_{\xi}^* (c_{\xi} v_{1,\xi}^l - c_{\xi}^* u_{1,\xi}^l), \quad (4d)$$

where $\mathcal{U}_1 = 2U_{11}(n_{1\xi}^c + \tilde{n}_{1\xi}) + U_{12}(n_{2\xi}^c + \tilde{n}_{2\xi}) + (\epsilon_\xi^{(1)} - \mu_1)$ and $\mathcal{U}_2 = 2U_{22}(n_{2\xi}^c + \tilde{n}_{2\xi}) + U_{12}(n_{1\xi}^c + \tilde{n}_{1\xi}) + (\epsilon_\xi^{(2)} - \mu_2)$ with $\underline{\mathcal{U}}_k = -\mathcal{U}_k$. To solve the above eigenvalue equation, we use a basis set of on-site Gaussian wave functions and define the quasiparticle amplitude as a linear combination of the basis functions. The condensate and noncondensate densities are then computed through the self-consistent solution of Eqs. (2) and (4). The noncondensate atomic density at the ξ th lattice site is

$$\tilde{n}_{k\xi} = \sum_l [(|u_{k\xi}^l|^2 + |v_{k\xi}^l|^2)N_0(E_l) + |v_{k\xi}^l|^2], \quad (5)$$

where $N_0(E_l) = (e^{\beta E_l} - 1)^{-1}$ with $\beta = (k_B T)^{-1}$ is the Bose-Einstein distribution factor of the l th quasiparticle mode with energy E_l at temperature T . The last term in $\tilde{n}_{k\xi}$ is independent of the temperature and, hence, represents the quantum fluctuations of the system. To examine the role of temperature we define the miscibility of the condensates in terms of the overlap integral

$$\Lambda = \frac{[\int n_1(\mathbf{r})n_2(\mathbf{r})d\mathbf{r}]^2}{[\int n_1^2(\mathbf{r})d\mathbf{r}][\int n_2^2(\mathbf{r})d\mathbf{r}]}. \quad (6)$$

Here, $n_k(\mathbf{r})$ is the total density of the k th condensate at position $\mathbf{r} \equiv (x, y)$. If the two condensates of the TBEC have complete overlap with each other, then the system is in the miscible phase with $\Lambda = 1$, whereas for the completely phase-separated case $\Lambda = 0$. Using Λ as a measure we identify the miscible and immiscible domains as a function of the temperature. As we use the coupled DNLSes to describe the TBEC, our study is valid deep within the superfluid domain, and the mean-field description would begin to deviate from the true results near the superfluid–Mott-insulator phase transition. In this regime a full quantum description [70] would be the appropriate method, and the same applies to probing the nature of the quantum phase transition [71–74]. It is well established that for some parameter regimes, TBECs in optical lattices can be either the superfluid phase of both species or the superfluid phase of one species coexisting with the Mott-insulator phase of the other [75–78].

B. Field-field correlation function

To define a measure of the coherence in the condensate we introduce the first-order correlation function $g_k^{(1)}(\mathbf{r}, \mathbf{r}')$, which can be expressed as expectations of the products of field operators at different positions and times [79–82]. These are normalized to obtain the unit modulus in the case of perfect coherence or a system consisting of only condensate atoms. Here, we restrict ourselves to ordered spatial correlation functions at a fixed and equal time. In terms of the quantum Bose field operator $\hat{\Psi}_k$ the first-order spatial correlation function is

$$g_k^{(1)}(\mathbf{r}, \mathbf{r}') = \frac{\langle \hat{\Psi}_k^\dagger(\mathbf{r})\hat{\Psi}_k(\mathbf{r}') \rangle}{\sqrt{\langle \hat{\Psi}_k^\dagger(\mathbf{r})\hat{\Psi}_k(\mathbf{r}) \rangle \langle \hat{\Psi}_k^\dagger(\mathbf{r}')\hat{\Psi}_k(\mathbf{r}') \rangle}}, \quad (7)$$

where $\langle \dots \rangle$ represents thermal average. It is important to note that the local first-order correlation function is equal to the density, i.e., $g_k^{(1)}(\mathbf{r}, \mathbf{r}) = n_k(\mathbf{r})$. The expression of $g_k^{(1)}(\mathbf{r}, \mathbf{r}')$ can

also be written in terms of condensate and noncondensate density correlations as

$$g_k^{(1)}(\mathbf{r}, \mathbf{r}') = \frac{n_k^c(\mathbf{r}, \mathbf{r}') + \tilde{n}_k(\mathbf{r}, \mathbf{r}')}{\sqrt{n_k(\mathbf{r})n_k(\mathbf{r}')}}, \quad (8)$$

where

$$\begin{aligned} n_k^c(\mathbf{r}, \mathbf{r}') &= \psi_k^*(\mathbf{r})\psi_k(\mathbf{r}'), \\ \tilde{n}_k(\mathbf{r}, \mathbf{r}') &= \sum_l [\{u_k^{*l}(\mathbf{r})u_k^l(\mathbf{r}') + v_k^{*l}(\mathbf{r})v_k^l(\mathbf{r}')\}N_0(E_l) \\ &\quad + v_k^{*l}(\mathbf{r})v_k^l(\mathbf{r}')], \\ n_k(\mathbf{r}) &= n_k^c(\mathbf{r}) + \tilde{n}_k(\mathbf{r}) \end{aligned}$$

are the condensate density correlation, noncondensate density correlation, and total density of the k th species, respectively. In the above expressions, $n_k^c(\mathbf{r}, \mathbf{r}')$ and $\tilde{n}_k(\mathbf{r}, \mathbf{r}')$ are obtained by expanding the complex amplitudes (c_ξ, d_ξ) and the quasiparticle amplitudes ($u_{k,\xi}^l, v_{k,\xi}^l$) in the localized Gaussian basis. At $T = 0$ K, the entire condensate cloud has complete coherence, and therefore $g_k^{(1)} = 1$ within the condensate region. In TBECs, the transition from the phase-separated to the miscible domain at $T \neq 0$ has characteristic signatures in the spatial structure of $g_k^{(1)}(\mathbf{r}, \mathbf{r}')$.

C. Numerical methods

To solve the coupled DNLSes, Eqs. (2), we scale and rewrite the equations in the dimensionless form. For this we choose the characteristic length scale as the lattice constant $a = \lambda_L/2$, with λ_L the wavelength of the laser which creates the lattice potential. Similarly, the recoil energy $E_R = \hbar^2 k_L^2/2m$, with m the atomic mass of the species and $k_L = 2\pi/\lambda_L$, is chosen as the energy scale of the system. We use the fourth-order Runge-Kutta method to solve these equations for zero as well as finite temperatures. To initiate the iterative steps to solve the equations appropriate initial guess values of c_ξ and d_ξ are chosen. For the present work we chose values corresponding to the side-by-side profile, as it gives quasiparticle energies which are real and not complex. This is important, as it shows that the solution we obtain is a stable one, and not a metastable one. The stationary ground-state wave function of the TBEC is obtained through imaginary-time propagation. In the tight-binding limit, the width of the orthonormalized Gaussian basis functions localized at each lattice site is $0.3a$. Furthermore, to study the quasiparticle excitation spectrum, we cast Eqs. (4) as matrix eigenvalue equations, and diagonalize the matrix using the routine ZGEEV from the LAPACK library [83]. For finite-temperature computations, to take into account thermal fluctuations, we solve the coupled equations, Eqs. (2) and Eqs. (4), self-consistently. The solution of the DNLSes is iterated until it satisfies the convergence criteria in terms of the number of condensate and noncondensate atoms. In general, the convergence is not smooth, and most of the time we encounter severe oscillations in the number of atoms. To remedy these oscillations and attain convergence, we damp the solution using the successive overrelaxation (underrelaxation) technique while updating the condensate (noncondensate)

atoms. Thus, the new solutions after an iteration cycle (IC) are

$$c_{\xi,IC}^{\text{new}} = r^{\text{ov}} c_{\xi,IC}^{\text{ov}} + (1 - r^{\text{ov}}) c_{\xi,IC-1}^{\text{ov}}, \quad (9a)$$

$$d_{\xi,IC}^{\text{new}} = r^{\text{ov}} d_{\xi,IC}^{\text{ov}} + (1 - r^{\text{ov}}) d_{\xi,IC-1}^{\text{ov}}, \quad (9b)$$

$$\tilde{n}_{k\xi,IC}^{\text{new}} = r^{\text{un}} \tilde{n}_{k\xi,IC}^{\text{un}} + (1 - r^{\text{un}}) \tilde{n}_{k\xi,IC-1}^{\text{un}}, \quad (9c)$$

where $r^{\text{ov}} > 1$ ($r^{\text{un}} < 1$) is the overrelaxation (underrelaxation) parameter. The choice of r^{ov} and r^{un} depend on the temperature and interaction parameters. In general, our observation is that the oscillations are more prominent at higher temperatures, and hence, lower values of r^{ov} and r^{un} must be chosen. This in turn implies that it takes a larger number of iterations to get converged solutions at higher temperatures.

III. RESULTS AND DISCUSSION

To examine the effects of thermal fluctuations on the quasiparticle spectra we consider the ^{87}Rb - ^{85}Rb TBEC with ^{87}Rb labeled species 1 and ^{85}Rb labeled species 2. The radial trapping frequencies of the harmonic potential are $\omega_x = \omega_y = \omega_{\perp} = 2\pi \times 50$ Hz with the anisotropy parameter $\omega_z/\omega_{\perp} = 20.33$, and these parameters are chosen based on the experimental work of Gadway and collaborators [34] on the TBEC of two hyperfine states of ^{87}Rb in optical lattices. It is important to note that we consider equal background trapping potentials for species 1 and 2. We emphasize here that the results are equally applicable to the case of the TBEC consisting of two hyperfine states of ^{87}Rb , however, we have chosen ^{87}Rb - ^{85}Rb to highlight that the small mass difference has no influence on the geometry of the ground state. The laser wavelength used to create the 2D lattice potential and the lattice depth are $\lambda_L = 1064$ nm and $V_0 = 5E_R$, respectively. We then take the total number of atoms as $N_1 = N_2 = 100$ confined in a 40×40 quasi-2D lattice system. It must be mentioned that the number of lattice sites considered is much larger than the spatial extent of the condensate cloud. Although the computations require a longer time with the larger lattice size, we chose it to ensure that the spatial extent of the thermal component is confined well within the lattice considered. The tunneling matrix elements are $J_1 = 0.66E_R$ and $J_2 = 0.71E_R$, which correspond to an optical lattice potential with a depth of $5E_R$. The intraspecies and interspecies on-site interactions are set as $U_{11} = 0.07E_R$, $U_{22} = 0.02E_R$, and $U_{12} = 0.15E_R$, respectively. For this set of parameters the ground-state density distribution of ^{87}Rb - ^{85}Rb TBEC is phase separated with side-by-side geometry. This is a symmetry-broken profile where one species is placed to the left and the other to the right of the trap center along the y axis. The evolution of the ground state from the miscible to the side-by-side density profile due to a decrease in the U_{22} is reported in our previous work [37]. In the present work, we demonstrate the role of temperature in the phase-separated domain of the binary condensate.

A. Zero temperature

At zero temperature, in the phase-separated domain, the energetically preferable ground state of TBEC is the side-by-side geometry, which is reported in our previous work [37].

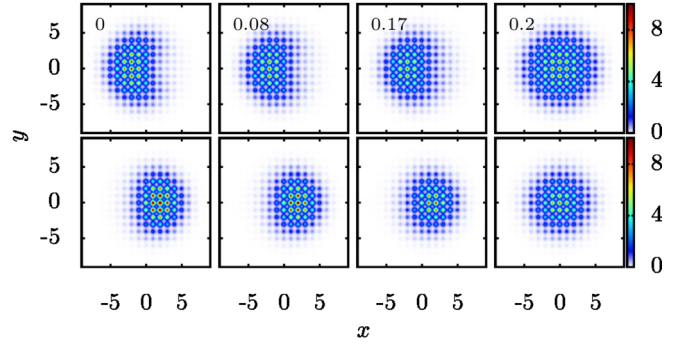


FIG. 1. Density distribution for the condensate atoms of ^{87}Rb - ^{85}Rb TBEC as a function of the temperature T/T_c . Density profiles of the ^{87}Rb (upper panel) and ^{85}Rb species (lower panel) are shown for $T/T_c = 0, 0.08, 0.17$, and 0.2 . In the phase-separated domain, the condensate density has side-by-side geometry at zero temperature, and as the temperature is increased, there is a transition to the miscible domain or the densities completely overlap at $T_{\text{ch}} = 0.185T_c$. Here x and y are measured in units of the lattice constant a .

Unlike in the 1D system [36] in the quasi-2D system the presence of the quantum fluctuations does not alter the ground state. For the parameters chosen the ^{87}Rb - ^{85}Rb TBEC is phase separated, and the overlap integral has the value $\Lambda = 0.10$. The density distributions of the condensate and noncondensate atoms of the two species at zero temperature are shown in Fig. 1 and Fig. 2. This is a symmetry-broken side-by-side geometry with noncondensate atoms more localized at the edges of the condensate along the y axis.

B. Finite temperatures

At $T \neq 0$, in addition to the quantum fluctuations, which are present at zero temperature, the thermal cloud also contributes to the noncondensate density. As shown in Figs. 1 and 2, at $T/T_c = 0.08$, the condensate density profiles of both species begin to overlap or, in other words, the two species are partly

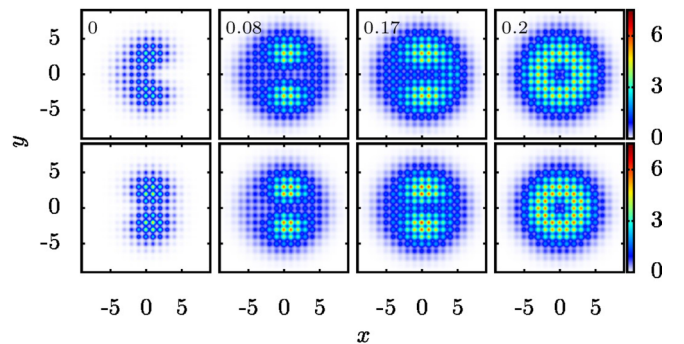


FIG. 2. Density distribution for the noncondensate atoms of ^{87}Rb - ^{85}Rb TBEC as a function of the temperature T/T_c . The noncondensate density of the ^{87}Rb (upper panel) and ^{85}Rb (lower panel) species are shown for $T/T_c = 0, 0.08, 0.17$, and 0.2 . Noncondensate atoms which are localized at the edges acquire rotational symmetry in the miscible phase, which happens at $T_{\text{ch}} = 0.185T_c$ as the temperature is increased. Here x and y are measured in units of the lattice constant a .

miscible. This is also evident from the value of $\Lambda = 0.16$, which shows a marginal increase compared to the value of 0.10 at zero temperature. In the figures, the temperature is defined in units of the critical temperature T_c of ^{87}Rb atoms, which for the parameters considered is 338 nK based on our finite-temperature computations. This value of T_c is consistent with the analytic expression for an ideal Bose gas in an optical lattice [84],

$$T_c = \frac{m\omega^2 a^2}{2\pi k_B} \left[\frac{N_k}{\zeta(3/2)} \right]^{2/3}, \quad (10)$$

where ω is the geometric mean of the three oscillator frequencies, N_k is the number of atoms of the k th species and $\zeta(3/2) = 2.612$ is the Riemann zeta function. In the presence of the harmonic confinement, the repulsive interatomic interaction reduces the density at the trap center and hence decreases T_c [84]. Upon a further increase in temperature, at $T/T_c = 0.18$, $\Lambda = 0.36$, this indicates an increase in the miscibility of the two species. Another important feature at $T/T_c = 0.08$ and 0.18 is the localization of the noncondensate atoms at the interface. This is due to repulsion from the condensate atoms and the lower thermal energy, which is insufficient to overcome this repulsion energy. The transition to the miscible domain occurs when the temperature exceeds the characteristic temperature

$$T_{\text{ch}} \approx \frac{\sqrt{n_{1\text{max}} n_{2\text{max}}} U_{12}}{k_B}, \quad (11)$$

where $n_{k\text{max}}$ is the maximum density of the k th species. At higher temperatures, the extent of overlap between the condensate density profiles increases, and the TBEC is completely miscible at $T_{\text{ch}} = 0.185T_c \approx 63$ nK. This is reflected in the value of $\Lambda = 0.95$, and the condensate as well as the noncondensate densities acquire rotational symmetry. The T_{ch} at which this transition occurs corresponds to the thermal energy $k_B T_{\text{ch}} = 0.72E_R$, which is comparable to the interspecies interaction energy of $0.66E_R$. Albeit, we discuss in detail the results for the parameters mentioned earlier, we find similar trends in the immiscible-miscible transition for different values of J 's and U 's. As is to be expected the only change is that the T_{ch} is lowered at a higher J ; hence the atoms require less thermal energy to overcome the interspecies repulsion energy for the transition to the miscible phase. In terms of the interaction energies, the lower value of U_{kk} and higher value of U_{12} increase the T_{ch} of the TBEC.

The transition from the phase-separated to the miscible domain can further be examined from the evolution of the quasiparticle modes as a function of the temperature. The evolution of the few low-lying mode energies with temperature is shown in Fig. 3, where the temperature is defined in units of T_c . It is evident from the figure that there are mode energy bifurcations with the increase in temperature. These are associated with the restoration of rotational symmetry when the TBEC is rendered miscible through an increase in the temperature.

As is to be expected the two lowest energy modes are the zero-energy or the Goldstone modes, which are the result of the spontaneous symmetry breaking associated with

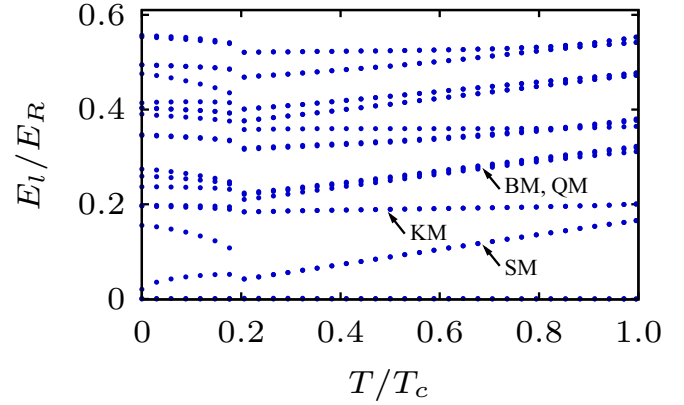


FIG. 3. Evolution of the excitation energies of the low-lying quasiparticle modes as a function of the temperature in ^{87}Rb - ^{85}Rb TBEC. The slosh and some of the other higher energy modes become degenerate at $T_{\text{ch}} = 0.185T_c$, where the density distribution is transformed from phase-separated to the miscible profile. In the plot, the slosh mode (SM), Kohn mode (KM), breathing mode (BM), and quadrupole mode (QM) are shown by the black arrows. Here, the excitation energy E_l and the temperature T are scaled with respect to the recoil energy E_R and the critical temperature T_c of the ^{87}Rb species, respectively.

condensation. In the phase-separated domain, these modes correspond to one each for each of the species. The first two excited modes are the nondegenerate Kohn or slosh modes of the two species, and these remain nondegenerate in the domain $T < T_{\text{ch}}$. The structures of these modes are shown in Figs. 4 and 5. When $T \geq T_{\text{ch}}$ as the TBEC acquires rotational symmetry, the slosh modes becomes degenerate with $\pi/2$ rotation. A key feature in the quasiparticle mode evolution is that the energy of all the out-of-phase modes increases for $T \geq T_{\text{ch}}$, whereas all the in-phase modes remain steady. Here, out-of-phase and in-phase means that the amplitudes u_1 and

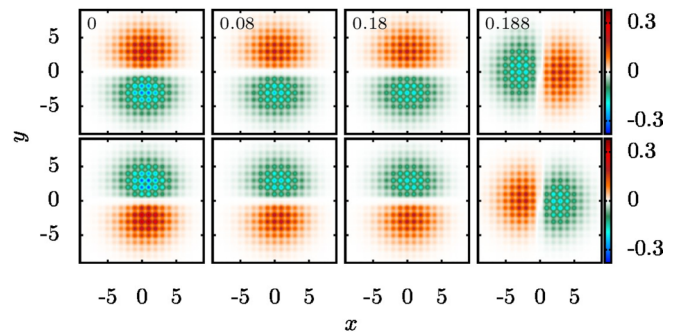


FIG. 4. Quasiparticle mode function of the first excited mode (slosh mode) as a function of the temperature for the ^{87}Rb - ^{85}Rb TBEC. The mode functions corresponding to the ^{87}Rb and ^{85}Rb species are shown in the upper and lower panels, respectively. The slosh mode is an out-of-phase mode where the density flows of the two species are in opposite directions. As the TBEC acquires rotational symmetry at $T_{\text{ch}} = 0.185T_c$, the slosh mode is rotated by an angle $\pi/2$ for $T/T_c \geq 0.185$. The value of T/T_c is shown in the top-left corner of each plot in the upper panel. The spatial coordinates x and y are in units of the lattice constant a .

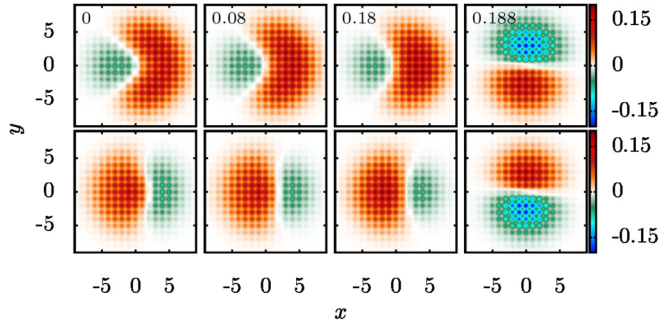


FIG. 5. Quasiparticle mode function corresponding to the second excited mode (slosh mode), which becomes degenerate with the first excited mode for $T/T_c \geq 0.185$. The mode functions of the ^{87}Rb and ^{85}Rb species are shown in the upper and lower panels, respectively. The value of T/T_c is shown in the top-left corner of each plot in the upper panel. Here x and y are in units of the lattice constant a .

u_2 of a quasiparticle are of different and the same phases, respectively. Among the low-energy modes, the Kohn mode is in-phase, whereas the breathing and quadrupole modes are out-of-phase in nature. One unique feature of the TBEC in the immiscible phase is the presence of interface modes; these have amplitudes prominent around the interface region. The existence of these modes is reported in our previous work [37] and was investigated in other works [85,86] for TBECs confined in a harmonic potential alone at zero temperature. As an example, one of the low-energy interface modes is shown in Fig. 6. It is evident from the figure that the mode is out-of-phase in nature, and it is transformed into the breathing mode in the miscible domain when $T \geq T_{\text{ch}}$. In the miscible domain, the breathing mode becomes degenerate with the quadrupole mode and gains energy. The quasiparticles of the miscible domain have a well-defined azimuthal quantum number, and modes undergo rotations as T is increased further.

To gain additional insight into the immiscible-miscible transition, we consider other TBECs. In particular, we consider

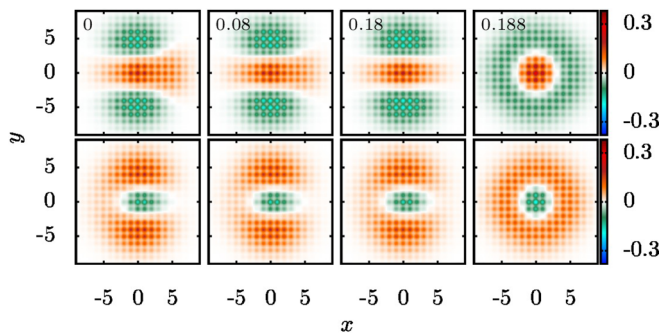


FIG. 6. The quasiparticle mode function corresponding to the interface mode in the phase-separated domain of ^{87}Rb - ^{85}Rb TBEC as a function of the temperature. This is an out-of-phase mode and the mode function is more prominent at the interface region between the condensates. For $T/T_c \geq 0.185$, when the TBEC acquires rotational symmetry, this mode is transformed into the out-of-phase breathing mode, where the mode functions are radially symmetric. The value of T/T_c is shown in the top-left corner of each plot in the upper panel. Here x and y are in units of the lattice constant a .

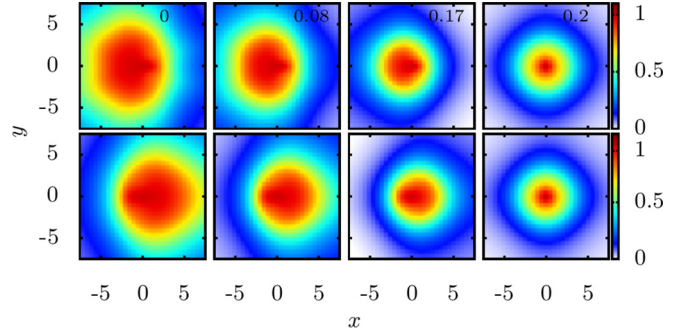


FIG. 7. Normalized first-order spatial correlation function $g_k^{(1)}(0, \mathbf{r})$ for ^{87}Rb (upper panel) and ^{85}Rb (lower panel) species at $T/T_c = 0, 0.08, 0.17,$ and 0.2 . Here x and y are measured in units of the lattice constant a .

Rb-Cs and Rb-K TBECs confined in quasi-2D optical lattices. The details of the parameters chosen and discussion are given in the Appendix. Starting from the immiscible domain we analyze the ground state and the quasiparticle mode evolution with increasing temperature. Based on the results we observe that the trend in the evolution of low-lying quasiparticle modes with the temperature is qualitatively similar to that of the ^{87}Rb - ^{85}Rb TBEC. The condensate density profiles also exhibit the same trend of transformation from immiscible side-by-side geometry to the rotationally symmetric miscible profile. As is to be expected, the value of T_{ch} depends on the mass ratio; this is due to the mass dependence of the interaction energy. In particular, for Rb-Cs and Rb-K TBECs, the T_{ch} values are $0.62T_c$ and $0.53T_c$, respectively. The thermal energies corresponding to these temperatures are $2.15E_R$ and $2.80E_R$, respectively. These are comparable to the interaction energies of the TBECs, which are $1.97E_R$ and $2.84E_R$, respectively. Here T_c is the critical temperature of condensation for the species with the lower value. In addition to the atomic mass of the condensates, as mentioned earlier, the immiscible-miscible transition also depends on the lattice parameters U and J . For these two TBECs also we have examined the density distributions with variation in the U and J parameters. We find similar trends in the value of T_{ch} as in the ^{87}Rb - ^{85}Rb TBEC. That is, a decrease in T_{ch} with an increase in J and an increase with lower and higher values of U_{kk} and U_{12} , respectively.

To investigate the spatial coherence of TBEC at equilibrium, we examine the trends in $g_k^{(1)}(0, \mathbf{r})$ defined earlier in Eq. (8) and shown in Fig. 7 for various temperatures. As mentioned earlier, at zero temperature, $n_k(\mathbf{r}) \approx n_k^c(\mathbf{r})$ has complete phase coherence, and therefore, $g_k^{(1)} = 1$ within the spatial extent of the condensates; this is shown in Fig. 7. At zero temperature or in the limit $\tilde{n}_k \equiv 0$ the correlation function, Eq. (8), resembles a Heaviside function, and the negligible contribution from the quantum fluctuations smooths out the sharp edges as $g_k^{(1)}$ drops to 0. More importantly, in the numerical computations this causes a loss of numerical accuracy, as it involves the division of two small numbers in Eq. (8) [87]. However, at a finite temperature the presence of noncondensate atoms modifies the nature of the spatial coherence present in the system. The decay rate of the correlation function increases with the temperature, and this

is evident in Fig. 7, which shows $g_k^{(1)}(0, \mathbf{r})$ at $T/T_c = 0.08$, 0.17, and 0.2. In addition to this, the transition from the phase-separated to the miscible TBEC is also reflected in the decay trends of $g_k^{(1)}(0, \mathbf{r})$.

IV. CONCLUSIONS

We have examined finite-temperature effects on the phenomenon of phase separation in TBECs confined in quasi-2D optical lattices. As the temperature is increased the phase-separated side-by-side ground-state geometry is transformed into the miscible phase. For the case of the TBEC comprised of ^{87}Rb and ^{85}Rb , the transformation occurs at the characteristic temperature. This demonstrates the importance of thermal fluctuations, which can make TBECs miscible. Based on the present work, in general, the TBEC undergoes the transition to the miscible phase at a characteristic temperature T_{ch} . This corresponds to the temperature at which the thermal energy overcomes the interspecies repulsion energy $\sqrt{n_{1\text{max}}n_{2\text{max}}}U_{12}$. The other key observation is that the transition from the phase-separated domain to the miscible domain is associated with a change in the nature of the quasiparticle energies. Low-lying out-of-phase modes, in particular, the slosh mode, become degenerate and increase in energy. On the other hand, in-phase modes, such as the Kohn mode, remain steady as the temperature ($T < T_c$) is increased. Interface modes, which are unique to the phase-separated domain, in addition to changing in energy are geometrically transformed into rotationally symmetric breathing modes in the miscible domain. The temperature-driven immiscible-to-miscible transition is also evident in the profile of the correlation functions.

ACKNOWLEDGMENTS

We thank A. Roy, S. Gautam, S. Bandyopadhyay, and R. Bai for useful discussions. The results presented in the paper are based on computations using Vikram-100, the 100TFLOP HPC Cluster at Physical Research Laboratory, Ahmedabad, India.

APPENDIX

Here, we provide brief descriptions of the computations pertaining to the Rb-Cs and Rb-K TBECs confined in quasi-2D optical lattices.

1. ^{87}Rb - ^{133}Cs TBEC

We consider a ^{87}Rb - ^{133}Cs TBEC containing 100 atoms of each species confined in a 40×40 quasi-2D optical lattice with a 1064-nm wavelength of the laser beams. The lower number of atoms is chosen to improve the convergence of finite-temperature computations, and at the same time it is sufficient to provide a good description of the superfluid phase of the TBECs. The radial trapping frequencies of the external harmonic trapping potential are $\omega_x = \omega_y = \omega_{\perp} = 2\pi \times 50$ Hz, with the anisotropy parameter 20.33 [34]. The tunneling matrix elements are $J_1 = 0.66E_R$ and $J_2 = 1.70E_R$, corresponding to a depth of the optical lattice $V_0 = 5E_R$. The lattice depth is considered such that the tight-binding limit, $V_0 \gg \mu_k$, is valid. The large difference in the values of J_k is due to the large mass difference between the atoms of the two species. The intraspecies and interspecies on-site interactions considered are $U_{11} = 0.96E_R$, $U_{22} = 0.42E_R$, and $U_{12} = 1.2E_R$. These DNLS parameters are derived from the intra- and interspecies scattering lengths of the species, the trap parameters, and the width of the Gaussian basis, which is $0.3a$. At zero temperature, the ground state of the TBEC has side-by-side geometry with $\Lambda = 0$ [37]. As in the case of ^{87}Rb - ^{85}Rb , as the temperature of the TBEC is increased ($T < T_c$), the system is transformed into the miscible phase. In addition, we have observed a bifurcation in the energy of the slosh mode, and the mode becomes degenerate with a discontinuity in the quasiparticle spectra at $T_{\text{ch}} = 0.62T_c \approx 140$ nK.

2. ^{87}Rb - ^{41}K TBEC

In the case of the ^{87}Rb - ^{41}K TBEC, the wavelength of the laser beams and the number of atoms are considered the same as in the case of the ^{87}Rb - ^{133}Cs TBEC. The radial trapping frequencies are $\omega_x = \omega_y = \omega_{\perp} = 2\pi \times 100$ Hz, with the anisotropy parameter 1.40 [88]. The tunneling matrix elements are $J_1 = 0.66E_R$ and $J_2 = 2.84E_R$, corresponding to a $5E_R$ lattice depth. The intraspecies and interspecies on-site interactions considered are $U_{11} = 0.20E_R$, $U_{22} = 0.06E_R$, and $U_{12} = 0.60E_R$. The set of parameters is chosen such that the density profile of the TBEC is immiscible and has side-by-side geometry at zero temperature. As in the previous cases, the geometry of the TBEC is transformed from the side-by-side type to the rotationally symmetric overlapping profile and the slosh mode becomes degenerate at $T_{\text{ch}} = 0.53T_c \approx 278$ nK.

-
- [1] D. Jaksch, C. Bruder, J. I. Cirac, C. W. Gardiner, and P. Zoller, *Phys. Rev. Lett.* **81**, 3108 (1998).
 - [2] C. Orzel, A. K. Tuchman, M. L. Fenselau, M. Yasuda, and M. A. Kasevich, *Science* **291**, 2386 (2001).
 - [3] M. Greiner, O. Mandel, T. Esslinger, T. W. Hänsch, and I. Bloch, *Nature (London)* **415**, 39 (2002).
 - [4] I. Bloch, J. Dalibard, and S. Nascimbène, *Nat. Phys.* **8**, 267 (2012).
 - [5] E. Demler and F. Zhou, *Phys. Rev. Lett.* **88**, 163001 (2002).
 - [6] A. B. Kuklov and B. V. Svistunov, *Phys. Rev. Lett.* **90**, 100401 (2003).
 - [7] A. Kuklov, N. Prokof'ev, and B. Svistunov, *Phys. Rev. Lett.* **92**, 050402 (2004).
 - [8] A. Pal and D. A. Huse, *Phys. Rev. B* **82**, 174411 (2010).
 - [9] S. Choi and L. Radzihovsky, *Phys. Rev. A* **84**, 043612 (2011).
 - [10] H.-F. Lin, H.-D. Liu, H.-S. Tao, and W.-M. Liu, *Sci. Rep.* **5**, 9810 (2015).
 - [11] O. Jürgensen, K. Sengstock, and D.-S. Lühmann, *Sci. Rep.* **5**, 12912 (2015).
 - [12] S. Trotzky, P. Cheinet, S. Fölling, M. Feld, U. Schnorrberger, A. M. Rey, A. Polkovnikov, E. A. Demler, M. D. Lukin, and I. Bloch, *Science* **319**, 295 (2008).

- [13] J. Simon, W. S. Bakr, R. Ma, M. E. Tai, P. M. Preiss, and M. Greiner, *Nature (London)* **472**, 307 (2011).
- [14] I. Bloch, *Nature (London)* **453**, 1016 (2008).
- [15] M. Lewenstein, A. Sanpera, V. Ahufinger, B. Damski, A. Sen(De), and U. Sen, *Adv. Phys.* **56**, 243 (2007).
- [16] I. Bloch, J. Dalibard, and W. Zwerger, *Rev. Mod. Phys.* **80**, 885 (2008).
- [17] T. Mishra, R. V. Pai, and B. P. Das, *Phys. Rev. A* **76**, 013604 (2007).
- [18] F. Zhan and I. P. McCulloch, *Phys. Rev. A* **89**, 057601 (2014).
- [19] M. Greiner, I. Bloch, O. Mandel, T. W. Hänsch, and T. Esslinger, *Phys. Rev. Lett.* **87**, 160405 (2001).
- [20] T. Roscilde and J. I. Cirac, *Phys. Rev. Lett.* **98**, 190402 (2007).
- [21] P. Buonsante, S. M. Giampaolo, F. Illuminati, V. Penna, and A. Vezzani, *Phys. Rev. Lett.* **100**, 240402 (2008).
- [22] G. Ceccarelli, J. Nespolo, A. Pelissetto, and E. Vicari, *Phys. Rev. A* **92**, 043613 (2015).
- [23] G. Ceccarelli, J. Nespolo, A. Pelissetto, and E. Vicari, *Phys. Rev. A* **93**, 033647 (2016).
- [24] T.-L. Ho and V. B. Shenoy, *Phys. Rev. Lett.* **77**, 3276 (1996).
- [25] E. Timmermans, *Phys. Rev. Lett.* **81**, 5718 (1998).
- [26] B. D. Esry and C. H. Greene, *Phys. Rev. A* **59**, 1457 (1999).
- [27] L. Wen, W. M. Liu, Y. Cai, J. M. Zhang, and J. Hu, *Phys. Rev. A* **85**, 043602 (2012).
- [28] S. B. Papp, J. M. Pino, and C. E. Wieman, *Phys. Rev. Lett.* **101**, 040402 (2008).
- [29] S. Tojo, Y. Taguchi, Y. Masuyama, T. Hayashi, H. Saito, and T. Hirano, *Phys. Rev. A* **82**, 033609 (2010).
- [30] D. J. McCarron, H. W. Cho, D. L. Jenkin, M. P. Köppinger, and S. L. Cornish, *Phys. Rev. A* **84**, 011603 (2011).
- [31] G. V. Chester, *Phys. Rev.* **100**, 446 (1955).
- [32] M. D. Miller, *Phys. Rev. B* **18**, 4730 (1978).
- [33] J. Catani, L. De Sarlo, G. Barontini, F. Minardi, and M. Inguscio, *Phys. Rev. A* **77**, 011603 (2008).
- [34] B. Gadway, D. Pertot, R. Reimann, and D. Schneble, *Phys. Rev. Lett.* **105**, 045303 (2010).
- [35] P. Soltan-Panahi, J. Struck, P. Hauke, A. Bick, W. Plenkers, G. Meineke, C. Becker, P. Windpassinger, M. Lewenstein, and K. Sengstock, *Nat. Phys.* **7**, 434 (2011).
- [36] K. Suthar, A. Roy, and D. Angom, *Phys. Rev. A* **91**, 043615 (2015).
- [37] K. Suthar and D. Angom, *Phys. Rev. A* **93**, 063608 (2016).
- [38] F. Lingua, M. Guglielmino, V. Penna, and B. Capogrosso Sansone, *Phys. Rev. A* **92**, 053610 (2015).
- [39] P. N. Galteland, E. Babaev, and A. Sudbø, *New J. Phys.* **17**, 103040 (2015).
- [40] O. E. Alon, A. I. Streltsov, and L. S. Cederbaum, *Phys. Rev. Lett.* **97**, 230403 (2006).
- [41] O. E. Alon, A. I. Streltsov, and L. S. Cederbaum, *Phys. Rev. A* **76**, 013611 (2007).
- [42] O. E. Alon, A. I. Streltsov, and L. S. Cederbaum, *Phys. Rev. A* **76**, 062501 (2007).
- [43] O. E. Alon, A. I. Streltsov, and L. S. Cederbaum, *Phys. Rev. A* **77**, 033613 (2008).
- [44] L. S. Cederbaum, A. I. Streltsov, Y. B. Band, and O. E. Alon, *Phys. Rev. Lett.* **98**, 110405 (2007).
- [45] P. Öhberg, *Phys. Rev. A* **61**, 013601 (1999).
- [46] H. Shi, W.-M. Zheng, and S.-T. Chui, *Phys. Rev. A* **61**, 063613 (2000).
- [47] K. Nho and D. P. Landau, *Phys. Rev. A* **76**, 053610 (2007).
- [48] A. Roy and D. Angom, *Phys. Rev. A* **92**, 011601 (2015).
- [49] N. P. Proukakis, *Phys. Rev. A* **74**, 053617 (2006).
- [50] S. Dettmer, D. Hellweg, P. Ryytty, J. J. Arlt, W. Ertmer, K. Sengstock, D. S. Petrov, G. V. Shlyapnikov, H. Kreutzmann, L. Santos, and M. Lewenstein, *Phys. Rev. Lett.* **87**, 160406 (2001).
- [51] D. Hellweg, L. Cacciapuoti, M. Kottke, T. Schulte, K. Sengstock, W. Ertmer, and J. J. Arlt, *Phys. Rev. Lett.* **91**, 010406 (2003).
- [52] S. Richard, F. Gerbier, J. H. Thywissen, M. Hugbart, P. Bouyer, and A. Aspect, *Phys. Rev. Lett.* **91**, 010405 (2003).
- [53] J. Esteve, J.-B. Trebbia, T. Schumm, A. Aspect, C. I. Westbrook, and I. Bouchoule, *Phys. Rev. Lett.* **96**, 130403 (2006).
- [54] T. Plisson, B. Allard, M. Holzmann, G. Salomon, A. Aspect, P. Bouyer, and T. Bourdel, *Phys. Rev. A* **84**, 061606 (2011).
- [55] O. Penrose and L. Onsager, *Phys. Rev.* **104**, 576 (1956).
- [56] E. A. Burt, R. W. Ghrist, C. J. Myatt, M. J. Holland, E. A. Cornell, and C. E. Wieman, *Phys. Rev. Lett.* **79**, 337 (1997).
- [57] B. Laburthe Tolra, K. M. O'Hara, J. H. Huckans, W. D. Phillips, S. L. Rolston, and J. V. Porto, *Phys. Rev. Lett.* **92**, 190401 (2004).
- [58] M. L. Chiofalo, M. Polini, and M. P. Tosi, *Eur. Phys. J. D* **11**, 371 (2000).
- [59] A. Smerzi and A. Trombettoni, *Phys. Rev. A* **68**, 023613 (2003).
- [60] M. P. A. Fisher, P. B. Weichman, G. Grinstein, and D. S. Fisher, *Phys. Rev. B* **40**, 546 (1989).
- [61] E. Lundh and J.-P. Martikainen, *Phys. Rev. A* **85**, 023628 (2012).
- [62] P. P. Hofer, C. Bruder, and V. M. Stojanović, *Phys. Rev. A* **86**, 033627 (2012).
- [63] A. Griffin, *Phys. Rev. B* **53**, 9341 (1996).
- [64] A. M. Rey, Ph.D. thesis, University of Maryland, 2004.
- [65] N. Elstner and H. Monien, *Phys. Rev. B* **59**, 12184 (1999).
- [66] S. Wessel, F. Alet, M. Troyer, and G. G. Batrouni, *Phys. Rev. A* **70**, 053615 (2004).
- [67] B. Capogrosso-Sansone, Ş. G. Söyler, N. Prokof'ev, and B. Svistunov, *Phys. Rev. A* **77**, 015602 (2008).
- [68] F. Gerbier, *Phys. Rev. Lett.* **99**, 120405 (2007).
- [69] E. Toth and P. B. Blakie, *Phys. Rev. A* **83**, 021601 (2011).
- [70] S. Klaiman, A. I. Streltsov, and O. E. Alon, *Chem. Phys.* **482**, 362 (2017).
- [71] W. Krauth, M. Caffarel, and J.-P. Bouchaud, *Phys. Rev. B* **45**, 3137 (1992).
- [72] V. A. Kashurnikov and B. V. Svistunov, *Phys. Rev. B* **53**, 11776 (1996).
- [73] M. Capello, F. Becca, M. Fabrizio, and S. Sorella, *Phys. Rev. Lett.* **99**, 056402 (2007).
- [74] S. Ramanan, T. Mishra, M. S. Luthra, R. V. Pai, and B. P. Das, *Phys. Rev. A* **79**, 013625 (2009).
- [75] V. A. Kashurnikov, N. V. Prokof'ev, and B. V. Svistunov, *Phys. Rev. A* **66**, 031601 (2002).
- [76] A. Isacsson, M.-C. Cha, K. Sengupta, and S. M. Girvin, *Phys. Rev. B* **72**, 184507 (2005).
- [77] R. A. Barankov, C. Lannert, and S. Vishveshwara, *Phys. Rev. A* **75**, 063622 (2007).
- [78] K. Mitra, C. J. Williams, and C. A. R. Sá de Melo, *Phys. Rev. A* **77**, 033607 (2008).
- [79] R. J. Glauber, *Phys. Rev.* **131**, 2766 (1963).
- [80] M. Naraschewski and R. J. Glauber, *Phys. Rev. A* **59**, 4595 (1999).
- [81] A. Bezett, E. Toth, and P. B. Blakie, *Phys. Rev. A* **77**, 023602 (2008).
- [82] A. Bezett and E. Lundh, *J. Phys. B* **45**, 205301 (2012).

- [83] E. Anderson, Z. Bai, C. Bischof, S. Blackford, J. Demmel, J. Dongarra, J. D. Croz, A. Greenbaum, S. Hammarling, A. McKenney, and D. Sorensen, *LAPACK Users' Guide*, 3rd ed. (Society for Industrial and Applied Mathematics, Philadelphia, PA, 1999).
- [84] D. Baillie and P. B. Blakie, *Phys. Rev. A* **80**, 031603 (2009).
- [85] C. Ticknor, *Phys. Rev. A* **88**, 013623 (2013).
- [86] C. Ticknor, *Phys. Rev. A* **89**, 053601 (2014).
- [87] C. Gies and D. A. W. Hutchinson, *Phys. Rev. A* **70**, 043606 (2004).
- [88] G. Thalhammer, G. Barontini, L. De Sarlo, J. Catani, F. Minardi, and M. Inguscio, *Phys. Rev. Lett.* **100**, 210402 (2008).